HHS Public Access

Author manuscript

J Immunol Methods. Author manuscript; available in PMC 2020 September 13.

Published in final edited form as:

J Immunol Methods. 2018 February ; 453: 11–19. doi:10.1016/j.jim.2017.07.014.

Application of Phospho-CyTOF to Characterize Immune Activation in Patients with Sickle Cell Disease In An Ex Vivo Model of Thrombosis

Jeffrey Glassberg[1], **Adeeb H. Rahman**[2,3,4], **Mohammad Zafar**[5], **Caroline Cromwell**[6], **Alexa Punzalan**[1], **Juan Jose Badimon**[5], **Louis Aledort**[6]

[1]Department of Emergency Medicine, Icahn School of Medicine at Mount Sinai, 3 E. 101st St., New York, NY, USA.

[2]Precision Immunology Institute, Icahn School of Medicine at Mount Sinai, 1470 Madison Avenue, New York, NY, USA.

[3]Human Immune Monitoring Core, Icahn School of Medicine at Mount Sinai, 1470 Madison Avenue, New York, NY, USA.

[4]Department of Genetics and Genomic Sciences, The Icahn Institute for Genomics and Multiscale Biology, Icahn School of Medicine at Mount Sinai, 1468 Madison Avenue, New York, NY, USA.

[5]Department of Medicine, Cardiology, Icahn School of Medicine at Mount Sinai, 1428 Madison Avenue, New York, NY, USA.

[6]Department of Medicine, Hematology and Oncology, Icahn School of Medicine at Mount Sinai, 1470 Madison Avenue, New York, NY, USA.

Abstract

Sickle cell disease (SCD) is a genetic disease caused by mutations in the beta globin gene, and inflammation plays a key role in driving many aspects of disease pathology. Early immune activation is believed to be associated with hemodynamic stresses and thrombus formation as cells traffic through blood vessels. We applied an extracorporeal perfusion system to model these effects ex vivo, and combined this with a phosphor-CyTOF workflow to comprehensively evaluate single-cell signatures of early activation across all major circulating immune subsets. These approaches showed immune activation following passage through the perfusion chamber, most notably in monocytes, which exhibited platelet aggregation and significantly elevated expression of multiple phospho-proteins. Overall, these studies outline a robust and broadly applicable workflow to leverage phospho-CyTOF to characterize immune activation in response to ex vivo or in vivo perturbations and may facilitate identification of novel therapeutic targets in SCD and other inflammatory diseases.

Corresponding Author: Jeffrey Glassberg, MD, MA, 1 Gustave L. Levy Place, Box 1620, New York, NY 10029, Jeffrey.Glassberg@mountsinai.org, Phone: (908) 875-4748, Fax: (212) 426-1946.

Keywords

Thrombosis; Sickle Cell Disease; Mass Cytometry; Immunology; Signaling; Phospho-Protein

1. Introduction

Sickle Cell Disease (SCD) is a recessively inherited disorder caused by mutations of the beta globin gene. In the most severe form of SCD, Sickle Cell Anemia, both beta globin genes carry the glu-val substitution at codon 6 of the beta globin locus causing hemoglobin S to be produced exclusively instead of the wild-type hemoglobin A1. Hemoglobin S polymerizes when deoxygenated, forming long rods which damage the red cell membrane causing chronic hemolysis, reduced red cell lifespan and ultimately the clinical manifestations of SCD (most notably vaso-occlusion and organ damage).[1–4] While membrane damage by hemoglobin S polymers is the proximal event in SCD pathophysiology, inflammation is a key component in the development of vessel occlusion, thrombosis, and organ injury. Broad anti-inflammatory therapies, glucocorticoids, relieve SCD symptoms but precipitate severe rebound effects when discontinued and have substantial side effects.[5–7] Targeted anti-inflammatory therapies such as selectin inhibitors have shown more promise, but more research is needed to understand the role of inflammation in SCD to identify other targets of intervention.

Vaso-occlusion, the critical event which leads to the complications of SCD (including but not limited to stroke, pain and organ damage), is driven by two synergistic, interacting processes: inflammation and thrombosis. With hemoglobin S polymerization and red cell membrane damage as the inciting event, several downstream pathways become activated including “oxidative stress, nitric oxide (NO) depletion, endothelial dysfunction,”[8] inflammation and thrombosis. Inflammatory cytokines including endothelin1, p and e-selectins, and soluble vascular cell adhesion molecule are elevated in SCD and levels correlate directly with SCD morbidity.[9–12] Monocytes, neutrophils and iNKT cells have been implicated as key cell populations in mediating SCD vaso-occlusion.[13–16] Additionally there are abnormalities at almost every level of the hemostatic system in SCD (SCD is one of few conditions which manifests both arterial and venous thrombosis including small, medium and large vessels) with several potential points of interaction between hemostasis and immune activation. These abnormalities (including platelet activation, abnormal thrombin kinetics and fibrinolysis) appear to be caused by and to further amplify inflammation and vaso-occlusion in SCD.[17] The diffuse nature of the activation of inflammation and thrombosis in SCD (often referred to as “inflammatory soup”) is a barrier to identifying appropriate points for therapeutic intervention. Studies that identify the proximal steps of inflammatory and hemostatic activation may help to identify promising therapeutic targets.

By allowing the measurement of over 40 parameters in a single sample, mass cytometry (CyTOF) offers a powerful approach to dissect the phenotypic and functional heterogeneity of complex cell samples. In addition to allowing detailed characterization of cell populations on the basis of surface receptor expression patterns, CyTOF can also be used to evaluate

signaling pathways using antibodies targeting phosophorylated protein epitopes.[18] This approach, referred to as phospho-CyTOF, can offer a detailed dynamic characterization of the nature of immune activation. In the current study, we describe the application of phospho-CyTOF to human whole blood samples characterize early immune activation events in associated with shearing and thrombotic stimuli using an ex vivo model of thrombosis. These analyses may be valuable in better delineating inflammatory pathways underlying SCD pathophysiology, and may offer a means to identify therapeutic targets in SCD and other diseases. We believe that the methods described here can also be broadly adapted to perform detailed analyses of early immune activation in a wide range of experimental and clinical settings.

2. Material and Methods

2.1 Subjects and samples

The following study was approved by the Mount Sinai Institutional Review Board and written informed consent was obtained from all participants. This was a prospective experiment performed on 5 individuals with SCD. Two control cohorts were used; 23 age, gender and race matched individuals served as historical controls for clotting analyses and 4 unselected healthy donors served as controls for the immune activation CyTOF assays. The inclusion criteria were age greater than 18, confirmation of SCD status by hemoglobin electrophoresis. Individuals who were taking oral anticoagulants or antiplatelet medications were excluded, and individuals taking hydroxyurea were excluded. The median age of SCD patients was 28 (range 26–32) and the median age of controls was 57 (range 47–65) (table 3). Racial characteristics were different between SCD patients and healthy controls in the CyTOF experiments, with the controls being predominantly White and individuals with SCD being predominantly Black.

On the day of the study patients reported to the AtheroThrombosis Research Unit of Mount Sinai. Following placement of a peripheral intravenous catheter, blood samples for CyTOF studies were collected and study to assess thrombus formation (described below) was performed. The IV catheter was then removed followed by 30 minutes of clinical observation to ensure that there were no procedural complications.

2.2 Ex Vivo Chamber Assessment of Thrombus Formation

Thrombus formation was assessed using the Badimon Perfusion Chamber, an ex vivo model of thrombosis that measures the acutely formed, platelet-rich thrombus.[19] This model consists of three chambers in series, each containing a piece of porcine aorta stripped of the intimal layer. The shear rate of the first chamber was set at $212s^{1}$ while the remaining two were $1{,}690s^{1}$, mimicking venous and moderately stenotic arterial flow conditions, respectively. A peristaltic pump at the distal end of the setup drew blood directly from the vein using an intravenous catheter thereby avoiding the use of any anticoagulant. Blood was passed over pieces of porcine aorta at a constant rate of 10 ml/minute for a total of 5 minutes, followed by phosphate-buffered saline (PBS) flush (Figure 1). The tissues were then fixed in 4% paraformaldehyde, processed for slide preparation and stained with combined Masson’s trichrome elastin (CME). Image acquisition of the sections and

measurement of thrombus area was carried out using Image Pro Plus software (version 4.5) and the data averaged to generate one low-shear and one high-shear result per study participant.

2.3 ThromboElastoMetry (TEM)

The effects on hemostasis were assessed using ThromboElastoMetry (TEM) with ROTEM Gamma instrument (Pentapharm GmbH, Germany). The assay employs a disposable measurement cell with a fixed cup, in which the motion of a continuously oscillating pin is optically detected. Whole blood was added to the cup with recombinant tissue factor or partial thromboplastin phospholipid to assess tissue-factor pathway (exTEM) or contact-activation pathway (inTEM) activity, respectively. Increasing resistance to the motion of the oscillating pin from clotting blood is recorded by the instrument and reflects physiological events mediated by the interaction of platelets, coagulation factors and fibrinogen.

Tests were carried out according to the manufacturer's instructions. The parameters of Coagulation Time (CT), Clot Formation Rate (CFR) and Maximum Clot Firmness (MCF) were recorded. The CT, the latency from addition of the start reagent to blood until clot formation begins, is a reflection of functional coagulation factors involved in thrombin formation. CFR evaluates the kinetics after the CT of stable clot formation from both activated platelets and fibrin. MCF is the measure of clot firmness and stability and depends on platelets, fibrinogen and factor XIII.

2.4 Whole blood preservation and processing for phospho-CyTOF analysis

In order to assess the patterns of immune activation caused by the Badimon chamber, blood collected directly from the patient was compared to blood that passed through the Badimon chamber. To evaluate the kinetics of protein phosphorylation, paired pre- and post-chamber blood samples were incubated at room temperature in sodium heparin vacutainers and at defined time intervals (10, 30 and 60 minutes), 500uL aliquots of blood were removed and mixed with 700uL of Proteomic Stabilizer (Smart Tube Inc.) to fix the samples and preserve cellular phospho-protein signatures (Figure 1). The samples were incubated at room temperature for 10 minutes and then transferred to dry ice and placed into storage at −80°C within one hour of collection.

To facilitate sample processing and minimize batch effects, all six samples contributed by each patient (10, 30 and 60 minute timepoints for pre- and post-chamber blood samples) were barcoded and processed together as a single batch. On the day of staining, the preserved blood samples were thawed in an ice water bath for 15 mins. Each 1.2mL fixed whole blood sample was then mixed with 3mL of Thaw-Lyse buffer (Smart Tube Inc.) and incubated for 10 minutes at room temperature. Samples were centrifuged, supernatants were discarded, and the pellet was resuspended in an additional 10mL of Thaw-Lyse buffer and incubated for an additional 10 minutes at room temperature, and then washed with cell staining media (CSM, Fluidigm).

2.5 Barcoding and cell staining

Each sample was washed and then resuspended in 800uL of 1X Barcode Perm Buffer (Fluidigm Inc.). Compatible Pd-barcodes were thawed, resuspended in 100uL of 1X Barcode Perm Buffer and added to the samples. Samples were incubated on ice for 30 minutes, then washed in CSM and pooled as together. Each barcoded set of samples (corresponding to a 3mL starting blood volume) was first resuspended in 100uL of CSM containing 100U/mL heparin (Sigma) to block non-specific MaxPar Antibody binding.[20] A titrated surface antibody panel designed to allow identification of all major immune subsets (Table 1) was prepared in an additional 100uL of CSM, filtered through a 0.1 micron spin filter (Amicon) and added directly to the sample. Samples were stained for 30 minutes on ice, then washed with CSM and fixed with freshly diluted 2% formaldehyde (Electron Microscopy Sciences) in PBS to cross-link and preserve all surface antibodies. The samples were then washed and permeabilized by the addition of 1ml of ice-cold 100% methanol, added dropwise while vortexing. Samples were incubated on ice for 30 minutes (or transferred to −80°C for long term storage), after which they were washed twice with CSM and again resuspended in 100uL of CSM containing 100U/mL heparin. A titrated panel of validated antibodies against phospho-protein epitopes was prepared in an addition 100uL of CSM, filtered through a 0.1 micron spin filter (Amicon) and added directly to the sample and incubated for 30 minutes on ice. Samples were then washed with CSM and incubated for 30 minutes in freshly-diluted 2% formaldehyde in PBS containing 0.125nM Ir nucleic acid intercalator (Fluidigm). The samples were washed and stored as pellets in CSM until CyTOF acquisition.

2.6 CyTOF Data Acquisition

Immediately prior to acquisition, samples were washed once with PBS, once with deionized water and then counted and resuspended at a concentration of 1 million cells/ml in water containing a 1/20 dilution of EQ 4 Element Beads (Fluidigm). Following routine instrument tuning, the samples were acquired on a CyTOF2 Mass Cytometer equipped with e SuperSample fluidics system (Victorian Airships) to facilitate bulk sample acquisitions. Samples were acquired at a flow rate of 0.045ml/min and an event rate of <400 events per second.

2.7 CyTOF data analysis

CyTOF FCS files were first concatenated and normalized using the bead-based normalization tool in the Helios software (Fluidigm), the barcoded samples were automatically deconvoluted and cross-sample doublets were filtered using a Matlab-based debarcoding tool,[21] and the resulting files were uploaded to Cytobank for analysis. Cell events were identified as Ir191/193 positive events, and residual Ce140+ normalization beads were excluded. Gated singlets were analyzed using Spanning Tree Progression of Density Normalized Events (SPADE) to map the multi-dimensional data to 2-dimensional space. All the data files were analyzed in a single SPADE analysis to ensure a consistent tree structure for population identification and annotation. The cells were clustered only on the basis of surface antibody markers, and for each time point the pre-chamber sample was designated as a baseline sample to allow SPADE visualization of fold changes in protein

phosphorylation between corresponding pre- and post-sample pairs. Major immune populations were identified on the SPADE tree based on canonical marker expression patterns, and the frequency and median phosphoprotein signal intensity for all cells in each of these defined populations was exported for downstream statistical analyses.[22]

2.8 Statistical Theory/Calculations

Statistical analyses were performed using SAS 9.4 and SPSS version 24. Standard descriptive statistics are reported including means, standard deviations, medians, and proportions as appropriate. For bivariate comparisons, t-tests, chi-square tests and corresponding non-parametric tests are used as appropriate. To quantify the effect of the Badimon chamber on the degree of immune activation, a multi-variable generalized estimating equation with linear outcome distribution was used. The outcome (dependent) variable was the difference in immune activation between blood that did and did not pass through the Badimon chamber (e.g. change in pSTAT1 phosphorylation). The independent variable was cell type (neutrophils, eosinophils, etc). Other covariates which were adjusted for included the time that the sample was allowed to wait at room temperature prior to stabilization (10, 30 or 60 minutes), disease status (SCD or healthy control) and an adjustment for repeated measurements on the same individual. Thus, outcomes reported are, for each cell type, the adjusted change in protein phosphorylation associated with passing through the ex-vivo thrombosis chamber. Regression diagnostics and sensitivity analyses were performed to assess for collinearity and model fit and to assess the effect of outliers on results. To adjust for multiple comparisons in the CyTOF assays, the Holm procedure was applied. A separate regression was performed for each of 8 phosphoproteins thus the adjusted alpha levels for regressions ranged from 0.05 to 0.00625. The Holm procedure was also applied to the results of thromboelastography in which 28 different comparisons were performed resulting in alpha cutoffs ranging from 0.05 to 0.0018.

3. Results

3.1 Individuals with SCD exhibit larger thrombus area under low shear conditions in comparison to healthy controls

Clotting analyses were performed on 5 individuals with SCD (median age 29, range 26–32) and compared with a historical cohort of 23 age, race and gender matched healthy controls (median age 29, range 26–32) (table 2). Thrombus size was significantly larger for individuals with SCD under low shear conditions (6217 μm^2 vs. 7250 μm^2, $p = 0.001$, Mann-Whitney U). Figure 2 shows representative images of thrombus from SCD patients under low shear conditions for SCD (top) and controls (bottom). Significant differences in thrombus size were not observed under high shear conditions (table 2). After correction for multiple comparisons, significant differences were observed in the extrinsic pathway including longer coagulation time (102 vs 65 seconds, $p < 0.001$), a faster rate of clot formation once clotting began (maximum clot firmness time 1438 seconds vs. 1934 seconds, $p < 0.001$). In both the extrinsic and intrinsic pathway similar trends were observed (longer overall coagulation time but faster clotting and greater clot firmness once clotting began) with p values below 0.05 in non-parametric testing however after correction for multiple

comparisons, statistical significance was not reached. Results of additional thromboelastography and thromboelastometry tests are shown in table 2.

3.2 Identification of major immune subsets in preserved whole blood sample using CyTOF

To identify cell signaling pathways activated by fluid shear and thrombosis in SCD, we developed a panel of surface markers that allowed identification of all major circulating immune populations and was compatible with SmartTube-preserved whole blood (table 1). We applied these markers in a combined SPADE analysis of 3 paired pre- and post-perfusion chamber blood samples from three healthy controls and four individuals with SCD (Figure 3A). The SPADE analysis allowed visualization and identification of major immune populations on the basis of canonical marker expression patterns (Figure 3B), and an examination of overall cellular composition in each of the samples (Figure 3C). The resulting SPADE tree offers a detailed map of immune cell composition on which dynamic changes in cell activation state may be visualized.

3.3 Comprehensive evaluation of protein phosphorylation patterns across immune subsets

The SPADE tree allowed clear visualization of dynamic changes in phospho-protein expression in post chamber samples as shown in Figure 4A. Aggregate visualization and statistical analyses of all analyzed phospho-proteins across all defined immune subsets identified activation of several major signaling pathways. In both healthy controls and SCD patients, after statistical adjustment for covariates, passage through the thrombosis chamber resulted in significantly increased elevation of all measured phosphoproteins in monocytes with the exception of p-S6 in CD14 low monocytes (Fig 4B and C). Within monocytes, the largest levels of change caused by the chamber were observed for phosphoproteins p-p38, p-ERK1/2 and p-CREB. Furthermore, levels of activation increased with time-points 10, 30 and 60 minutes (i.e. the differences between pre and post chamber blood were larger for blood that was allowed to sit for longer before stabilization in buffer solution). Levels of pCREB within neutrophils were also higher after passing through the chamber (fold change = 0.25, 95% CI 0.16 – 0.33, $p < 0.000$) however these signals already reached maximal levels by 10 minutes and then remained constant over time. Importantly, these experiments were designed primarily to demonstrate the application of phospho-CyTOF to evaluate immune activation induced by the thrombosis chamber, and were not optimally designed or statistically powered to identify significant differences between SCD patients and controls. Thus, while numerical differences in phosphoprotein expression levels were observed between SCD and controls, these were not compared statistically.

3.4 Patients with SCD exhibit statistically significant increases in platelet monocyte aggregates in response to the ex-vivo perfusion chamber

Platelet events can be identified using CyTOF based on high CD61 expression levels. Most free platelets are excluded from this CyTOF analysis both due to losses during sample wash steps and restricting the SPADE analysis to Ir191/193 DNA-high nucleated cells. However, aggregation of platelets with other cell types can be identified based on increases in CD61 expression. Figure 5 illustrates the application of this method to pre- and post-chamber

samples, showing progressive fold-change increases in expression of CD61 within monocyte populations over time, indicating the formation of monocyte-platelet aggregates in response to the chamber (Fig. 5A). These changes are summarized for both SCD patients and healthy controls in Fig. 5B and C, respectively. In patients with SCD the fold change in CD61 on CD14hi monocytes was 1.32 (95%CI 0.59 – 2.05) and for CD14low monocytes was 1.06 (95%CI 0.18 – 1.94). For healthy controls, fold change in CD14 high and low monocytes was not statistically significant 0.49 (95%CI −0.12 – 1.11) and 0.17 (95%CI −0.03 – 0.38) respectively.

While these analyses demonstrate comprehensive evaluation of phospho-protein expression and platelet aggregates as individual parameters, one of the strengths of CyTOF analyses is that each of these parameters is measured simultaneously on a single cell basis, allowing an evaluation of relationships between them. For example, evaluating p-p38 together with p-CREB shows that phosphorylation of these proteins occurs in all CD14hi monocytes, with phosphorylation of p38 showing slightly faster kinetics than phosphorylation of CREB (Fig 5D). In contrast, when evaluating protein phosphorylation in relation to monocyte-platelet aggregation, it becomes clear that some monocyte-platelet aggregates exist at baseline, and that while the frequency of these aggregates increases over time, this occurs for only a subset of monocytes (Fig 5E). Furthermore, it appears that phosphorylation of p38 precedes the increase in the frequency of monocyte-platelet aggregate suggesting that the formation of platelet aggregates may be a consequence rather than a cause of monocyte activation in the thrombosis chamber.

4. Discussion

In this manuscript, we report the application of phospho-CyTOF to broadly assess the early single-cell signaling profile of immune activation in response to a thrombogenic stimulus. With the continuing emergence of data that interactions between the hemostatic and immune system drives pathophysiology of SCD and other disease states, our approach may be of great use. These experiments demonstrate the ability to quantify time-dependent immune activation in individuals with SCD after passage of blood through an ex vivo thrombosis chamber. Platelets have been increasingly implicated in SCD pathogenesis as mediators of vaso-occlusion and more recently as mediators of inflammation. Our finding that platelet-monocyte aggregates form intensely within minutes of exposure to the ex-vivo thrombosis chamber supports the role of platelets in SCD and identifies the platelet monocyte interaction as a potential target for intervention.

Cytometry experiments that quantify single cell expression levels of stable proteins can be very useful in characterizing the cellular heterogeneity of complex samples, but do not necessarily assess cell activation state. In contrast, phospho-flow, or the application of flow cytometry to quantify phosphorylation of tyrosine, serine and threonine residues, is useful to describe the control of protein activity in the activation of various cellular cascades, and offers insights into the dynamic activation state of individual cells[18,21,23]. This information can be useful in determining the key steps in cell signaling events, which can inform underlying mechanisms of activation and eventually lead to the development of targeted therapies to interrupt maladaptive cellular processes.[21] The adaptation of phospho-flow

methods to mass cytometry is novel and offers the advantages of simultaneously allowing the measurement of a much larger number of surface markers and phosphoproteins. This allows a more detailed description of the cellular composition of a sample (Fig. 3), potential interactions between cell types (Fig. 4), and a more comprehensive evaluation of the signaling pathways that may be induced within those populations (Fig. 5). The ability to measure more phospho-proteins reflecting activation of multiple different signaling pathways is particularly useful in exploratory studies such as those described in this manuscript.

Mass cytometry also offers the opportunity to leverage barcoding approaches for pooled sample analysis,[21,23,24] with commercially-available palladium-based barcoding kits (Fluidigm) allowing pooled processing of up to 20 samples at one time. This is a tremendously powerful approach that effectively eliminates any technical variation or batch effects that may arise during sample staining or CyTOF acquisition, which allows subtle changes in protein expression to be accurately compared across samples. This is particularly important in phospho-CyTOF experiments, since biologically relevant changes in phosphoprotein expression can often exhibit very small effect sizes, which can be difficult to distinguish from technical artifacts when samples are processed separately. The use of combinatorial barcoding schemes also offers the additional benefit of facilitating the identification and exclusion of cell-cell doublets. The approach described in this manuscript, which leverages SmartTube buffers to stabilize whole blood phosphoprotein signatures with minimal sample perturbation, and pooled barcoded analysis of complete sample batches, provides an optimal method to minimize technical variability and improve the robustness of phospho-protein measurements. As shown in figure 5, statistical significance was reached for several measurements where the observed fold change was quite small, and sensitivity analyses revealed that the reason for this was that the extremely low variability in the CyTOF results across different samples, which speaks to the high level of precision offered by this approach.

In this study, phospho-CyTOF offered an unprecedented high resolution evaluation of immune activation induced in an ex vivo model of thrombosis. We found evidence of activation of multiple immune cell types: most notably, monocytes that passed through the thrombosis chamber showed high levels of platelet aggregation and also showed elevated expression of all 8 measured phospho-proteins. These patterns of activation were observed both in samples from SCD patients and controls, suggesting that they largely reflect generalized immune activation induced by the perfusion chamber. We hypothesize that this immune activation may be driven by a combination of hemodynamic shear stresses, engagement of pattern recognition receptors (PRRs) by ligands in the chamber, and secondary autocrine and paracrine effects of induced cytokine secretion. Evaluating these potential mechanisms is the subject of future studies. While the degree of monocyte activation appeared to be more pronounced in SCD patients than controls, statistical validation of these findings and their clinical relevance require additional experiments with larger cohorts. However, these findings would support previous studies that have found that activated monocytes play a key role in the hyper-inflammatory phenotype of SCD, and may be a potential target for intervention.[24]

In summary, we report that within minutes of exposure of SCD blood to an ex vivo thrombosis chamber, monocytes become markedly activated, exhibiting phosphorylation of multiple signaling proteins and formation of monocyte-platelet aggregates. Our data outline a robust workflow to leverage phospho-CyTOF to evaluate early immune activation in response to ex vivo perturbation, and these methods can also be easily adapted to evaluate in vivo immune activation using minimally manipulated whole blood samples.[25] These findings are useful in delineating key cell signaling pathways and describing interactions between the immune and hemostatic systems, and these methods are widely adaptable characterize immune activation and identify potential therapeutic targets across multiple disease states. In SCD, the platelet-monocyte interaction requires further study to identify therapeutic targets.

Acknowledgements

We thank Oksana Mayovska, Xinzheng Guo and the Human Immune Monitoring Center for technical assistance. Funding for this study was provided internally by Dr. Louis Aledort.

Abbreviations

SCD	Sickle Cell Disease
TEM	ThromboElastoMetry
exTEM	extrinsic TEM
inTEM	intrinsic TEM

References

1. Ballas SK. Sickle cell anaemia: progress in pathogenesis and treatment. Drugs 2002;62:1143–72. [PubMed: 12010077]
2. Walmet PS, Eckman JR, Wick TM. Inflammatory mediators promote strong sickle cell adherence to endothelium under venular flow conditions. Am J Hematol 2003;73:215–24. [PubMed: 12879422]
3. Blann AD, Marwah S, Serjeant G, Bareford D, Wright J. Platelet activation and endothelial cell dysfunction in sickle cell disease is unrelated to reduced antioxidant capacity. Blood Coagul Fibrinolysis 2003;14:255–9. [PubMed: 12695748]
4. Hebbel RP, Osarogiagbon R, Kaul D. The endothelial biology of sickle cell disease: inflammation and a chronic vasculopathy. Microcirculation 2004;11:129–51. [PubMed: 15280088]
5. Strouse JJ, Takemoto CM, Keefer JR, Kato GJ, Casella JF. Corticosteroids and increased risk of readmission after acute chest syndrome in children with sickle cell disease. Pediatr Blood Cancer 2008;50:1006–12. [PubMed: 17849474]
6. Kumar R, Qureshi S, Mohanty P, Rao SP, Miller ST. A short course of prednisone in the management of acute chest syndrome of sickle cell disease. J Pediatr Hematol Oncol 2010;32:e91–4. [PubMed: 20216237]
7. Quinn CT, Stuart MJ, Kesler K, et al. Tapered oral dexamethasone for the acute chest syndrome of sickle cell disease. Br J Haematol 2011;155:263–7. [PubMed: 21848879]
8. Torres LS, Okumura JV, Silva DG, et al. Inflammation in Sickle Cell Disease: Differential and Down-Expressed Plasma Levels of Annexin A1 Protein. PLoS One 2016;11:e0165833. [PubMed: 27802331]
9. Duits AJ, Pieters RC, Saleh AW, et al. Enhanced levels of soluble VCAM-1 in sickle cell patients and their specific increment during vasoocclusive crisis. Clin Immunol Immunopathol 1996;81:96–8. [PubMed: 8808648]

10. Saleh AW, Hillen HF, Duits AJ. Levels of endothelial, neutrophil and platelet-specific factors in sickle cell anemia patients during hydroxyurea therapy. Acta Haematol 1999;102:31–7. [PubMed: 10473885]
11. Duits AJ, Rojer RA, van Endt T, et al. Erythropoiesis and serum sVCAM-1 levels in adults with sickle cell disease. Ann Hematol 2003;82:171–4. [PubMed: 12634950]
12. Schnog JB, Rojer RA, Mac Gillavry MR, Ten Cate H, Brandjes DP, Duits AJ. Steady-state sVCAM-1 serum levels in adults with sickle cell disease. Ann Hematol 2003;82:109–13. [PubMed: 12601490]
13. Field JJ, Nathan DG, Linden J. Targeting iNKT cells for the treatment of sickle cell disease. Clin Immunol 2011.
14. Frenette PS. Sickle cell vaso-occlusion: multistep and multicellular paradigm. Curr Opin Hematol 2002;9:101–6. [PubMed: 11844991]
15. Chang J, Shi PA, Chiang EY, Frenette PS. Intravenous immunoglobulins reverse acute vasoocclusive crises in sickle cell mice through rapid inhibition of neutrophil adhesion. Blood 2008;111:915–23. [PubMed: 17932253]
16. Hebbel RP, Schwartz RS, Mohandas N. The adhesive sickle erythrocyte: cause and consequence of abnormal interactions with endothelium, monocytes/macrophages and model membranes. Clin Haematol 1985;14:141–61. [PubMed: 3886233]
17. Lim MY, Ataga KI, Key NS. Hemostatic abnormalities in sickle cell disease. Curr Opin Hematol 2013;20:472–7. [PubMed: 23817169]
18. Bendall SC, Simonds EF, Qiu P, et al. Single-cell mass cytometry of differential immune and drug responses across a human hematopoietic continuum. Science 2011;332:687–96. [PubMed: 21551058]
19. Zafar MU, Vorchheimer DA, Gaztanaga J, et al. Antithrombotic effects of factor Xa inhibition with DU-176b: Phase-I study of an oral, direct factor Xa inhibitor using an ex-vivo flow chamber. Thromb Haemost 2007;98:883–8. [PubMed: 17938815]
20. Rahman AH, Tordesillas L, Berin MC. Heparin reduces nonspecific eosinophil staining artifacts in mass cytometry experiments. Cytometry A 2016;89:601–7. [PubMed: 27061608]
21. Zunder ER, Finck R, Behbehani GK, et al. Palladium-based mass tag cell barcoding with a doublet-filtering scheme and single-cell deconvolution algorithm. Nature protocols 2015;10:316–33. [PubMed: 25612231]
22. Qiu P, Simonds EF, Bendall SC, et al. Extracting a cellular hierarchy from high-dimensional cytometry data with SPADE. Nature biotechnology 2011;29:886–91.
23. Bodenmiller B, Zunder ER, Finck R, et al. Multiplexed mass cytometry profiling of cellular states perturbed by small-molecule regulators. Nature biotechnology 2012;30:858–67.
24. Fread KI, Strickland WD, Nolan GP, Zunder ER. An Updated Debarcoding Tool for Mass Cytometry with Cell Type-Specific and Cell Sample-Specific Stringency Adjustment. Pacific Symposium on Biocomputing Pacific Symposium on Biocomputing 2016;22:588–98.
25. Gaudilliere B, Fragiadakis GK, Bruggner RV, et al. Clinical recovery from surgery correlates with single-cell immune signatures. Science translational medicine 2014;6:255ra131.

Highlights

- Interactions between immune and hemostatic systems drive pathophysiology of SCD
- Phospho-CyTOF identified immune signatures in SCD after fluid shear thrombosis
- Platelet monocyte aggregates occur within minutes of ex-vivo thrombosis in SCD

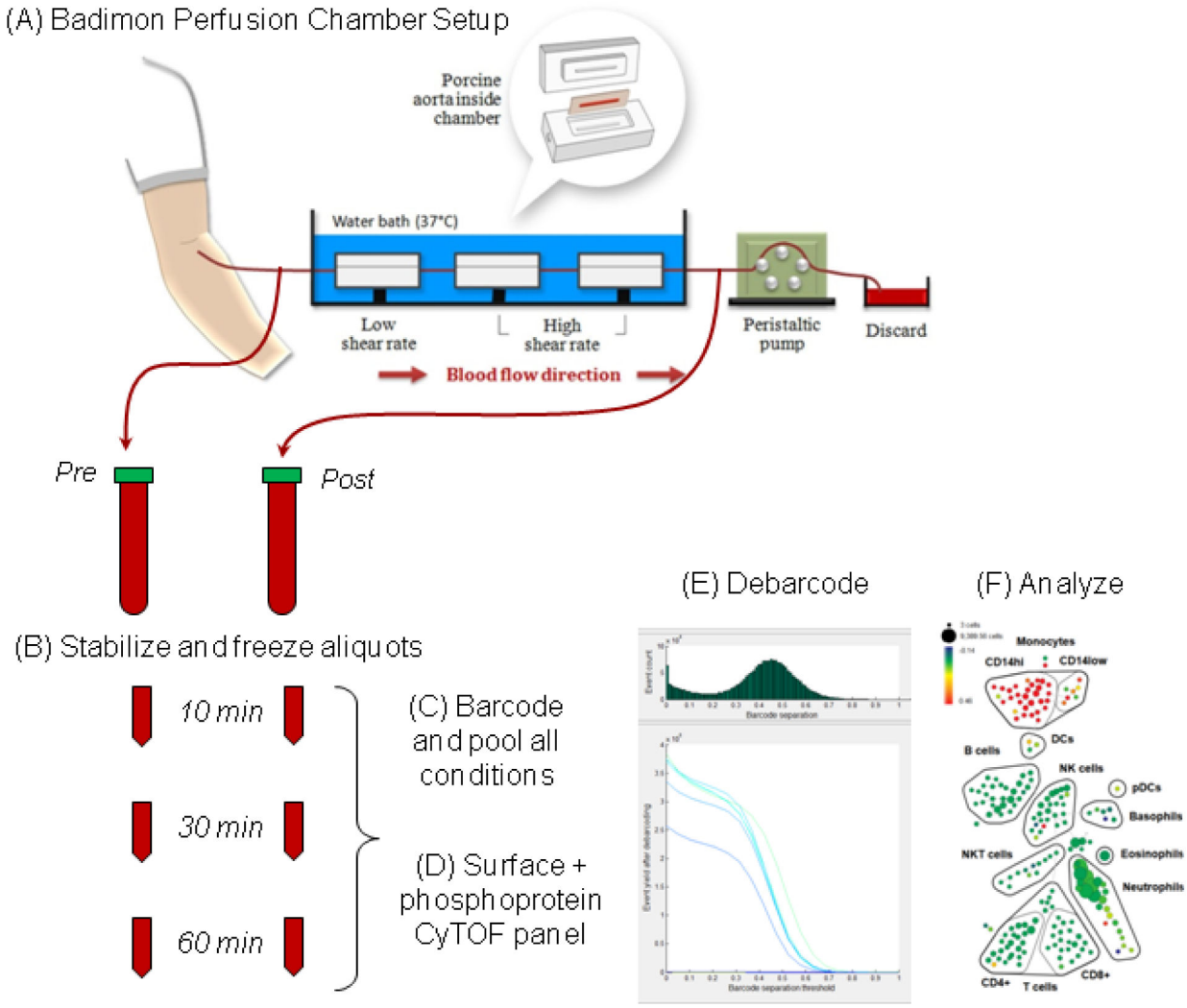

Figure 1. Schematic of Badimon Vortex – Phospho-CyTOF experiment.

An intravenous catheter was introduced and blood was drawn through a Badimon Perfusion Chamber using a peristaltic pump. Blood samples were collected before and after passing through the chamber in lithium heparin vacutainer tubes and incubated at room temperature. Aliquots were removed at 10, 30 or 60 minute intervals and stabilized and cyropreserved using SmartTube buffer. Batches of samples were thawed, barcoded and processed for phospho-CyTOF analysis.

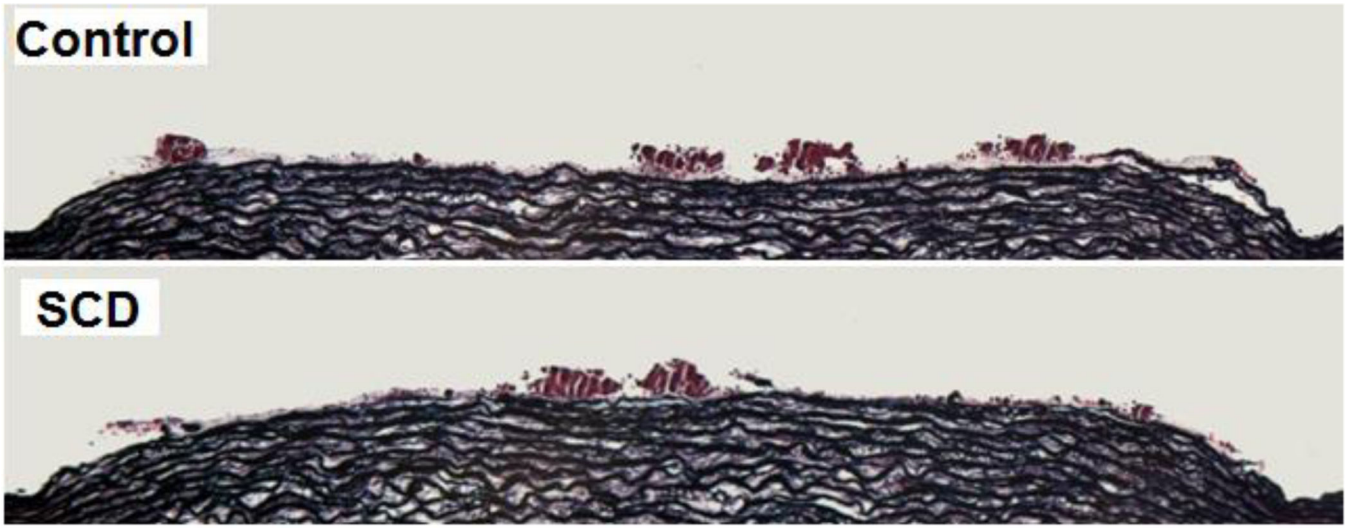

Figure 2. Evaluation of thrombus formation.

Representative image showing thrombus formation in the Badimon Perfusion Chamber under low-shear rate conditions for SCD patient (top) and control (bottom). The overall size of the platelet-rich thrombi formed was greater for SCD patients than the healthy controls.

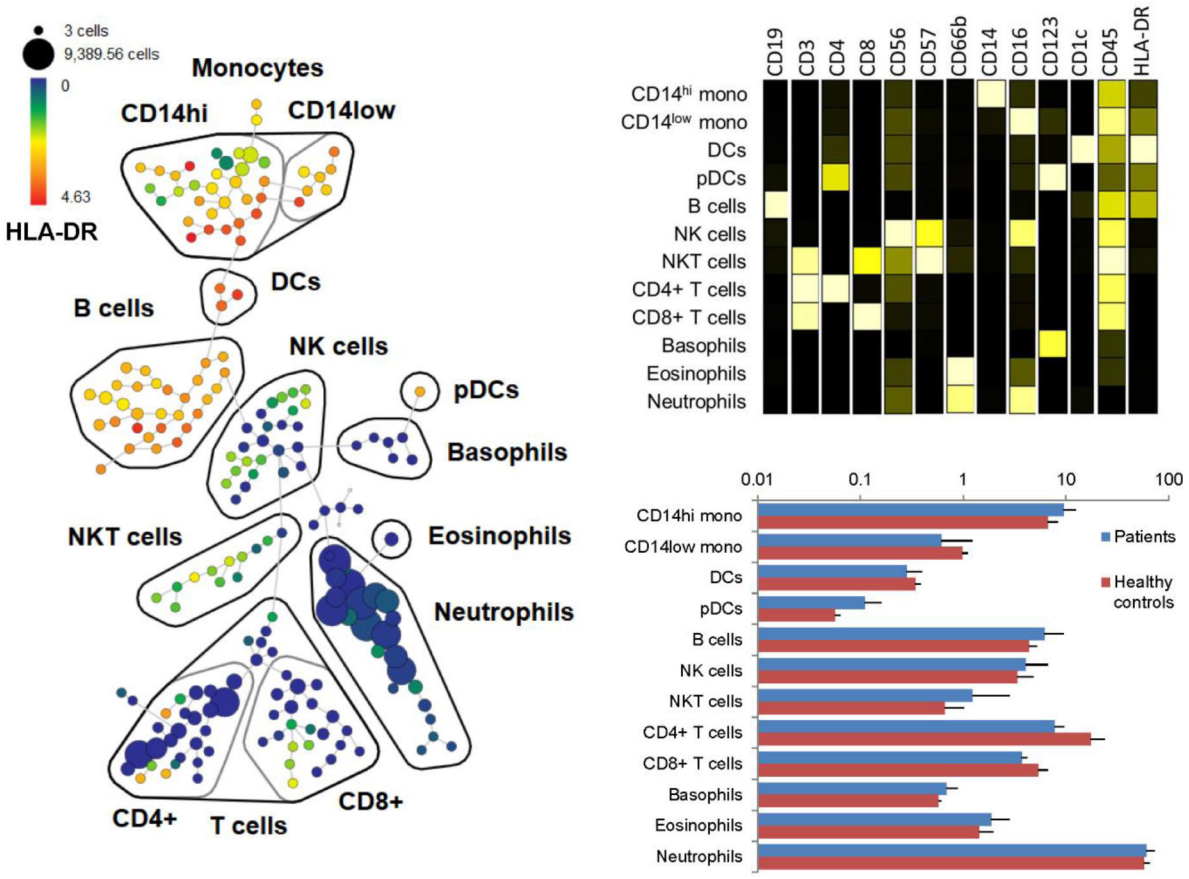

Figure 3. SPADE analysis of CyTOF data.

(A) Pooled CyTOF data were clustered using SPADE based on surface markers, and major immune subsets were identified and annotated based on canonical surface marker expression patterns. (B) Median surface marker expression profiles of identified immune populations. (C) Frequency of immune subsets in SCD patients (blue) and healthy controls (red).

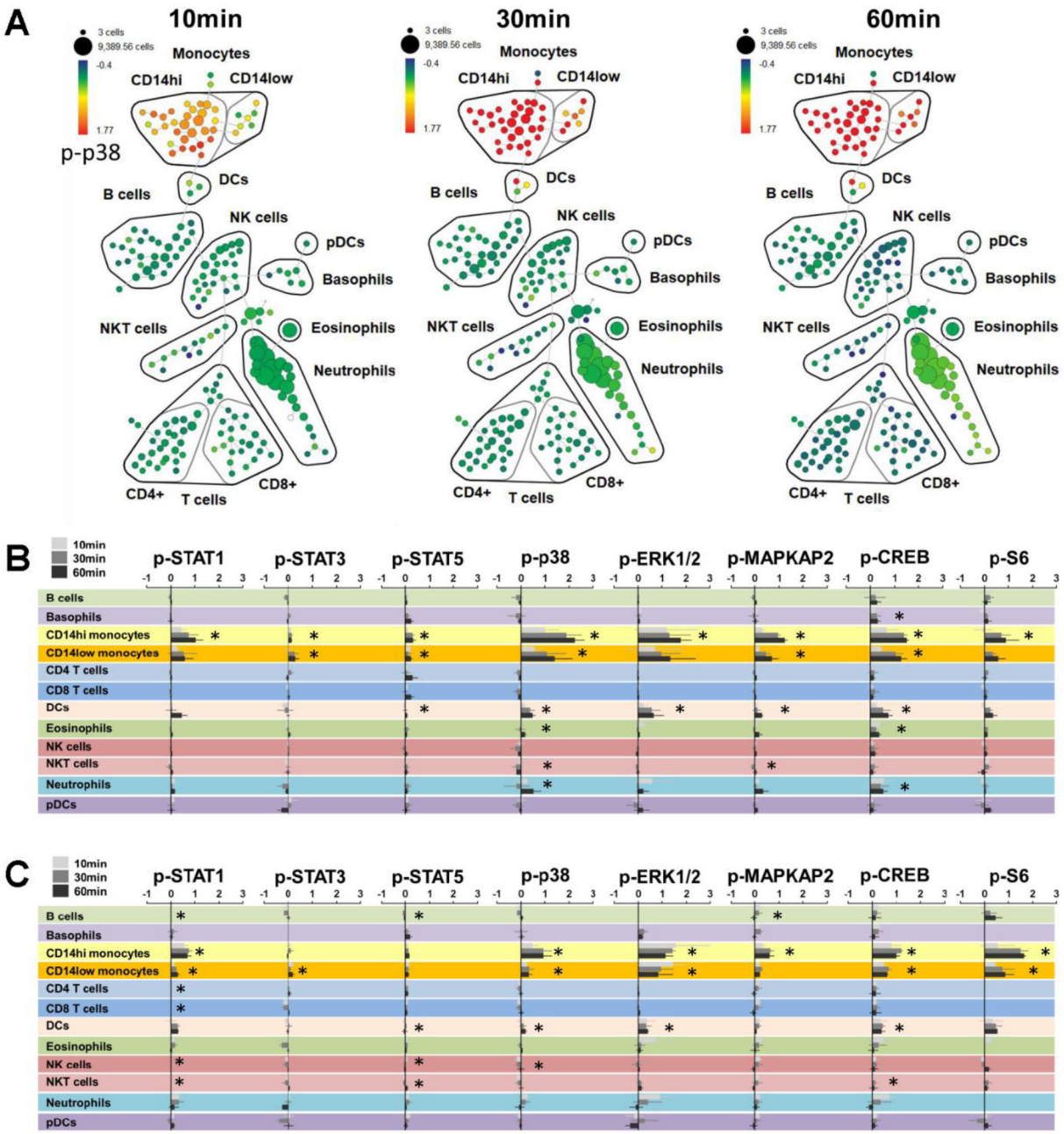

Figure 4. Analysis of phospho-protein activation.

(A) SPADE map of a representative set of SCD patient samples visualizing fold change expression of p-p38 in post-chamber samples relative to time-matched samples that did not pass through the chamber (average p-p38 fold change for CD14hi monocytes = 1.35 (95% CI 0.91 – 1.80, $p < 0.0001$). Summarized median fold change for all measured phospho proteins across all immune subsets over time for SCD patients (B) and healthy controls (C). Asterisks indicate statistically significant differences in expression of each phospho-protein within each cell population between pre- and post-chamber samples after adjustment for multiple comparisons using the Holm procedure. Hypotheses were tested using a

multivariable general estimating equation for each surface protein. Each regression included adjustment for time and cell type, with clustering of standard errors around each individual.

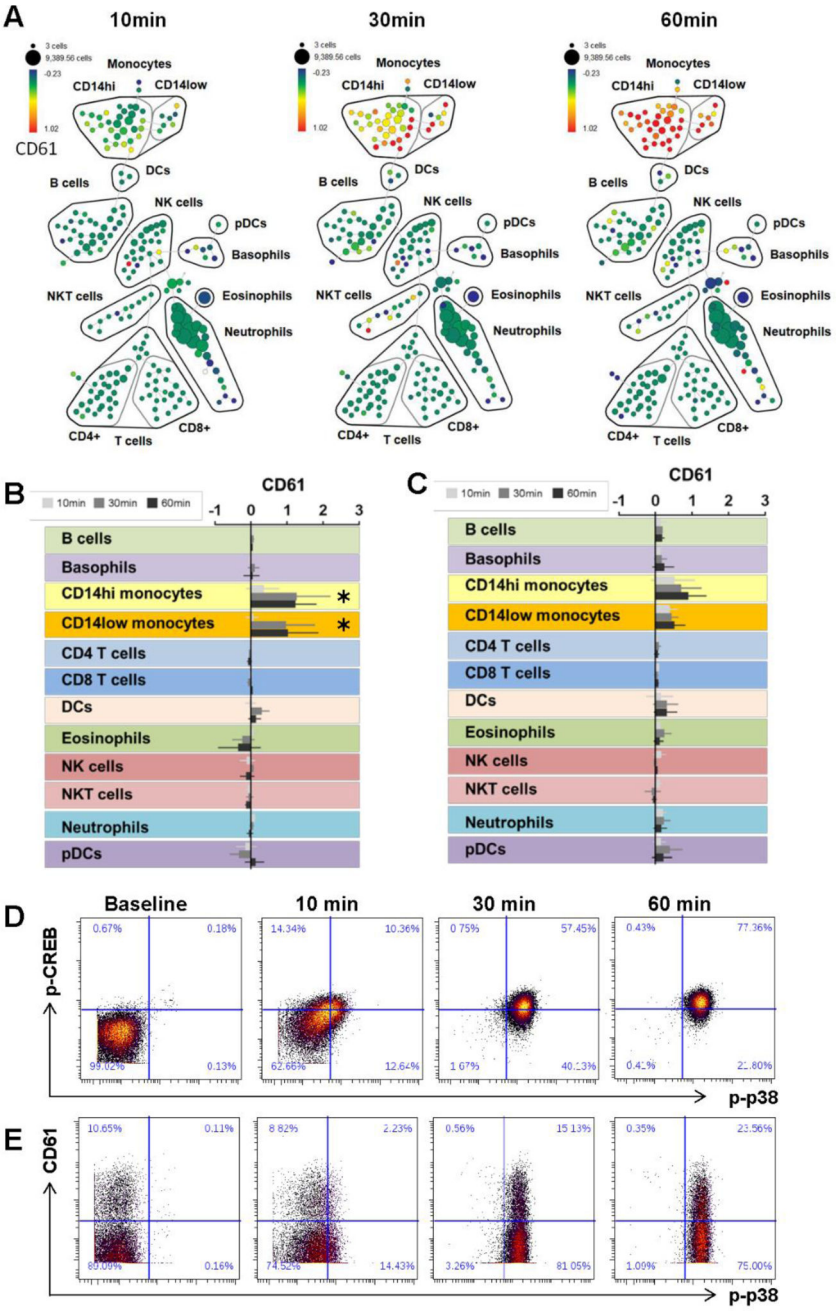

Figure 5. Analysis of immune cell-platelet aggregates.

Patients with SCD exhibit statistically significant increases in platelet monocyte aggregates in response to thrombosis whereas controls do not. (A) SPADE map of a representative set of SCD patient samples visualizing fold change expression of CD61 in post-chamber samples relative to time-matched samples that did not pass through the chamber. The median fold change in CD61 expression across all immune subsets over time are shown for SCD patients (B) and healthy controls (C). Asterisks denote statistically significant changes within a given cell population when comparing blood that passed through the thrombosis chamber to blood that was collected directly from the patient. (D) Biaxial plots of a

representative patient sample showing single cell expression of p-p38 vs. p-CREB on gated CD14hi monocytes post chamber. (E) Biaxial plots of a representative patient sample showing single cell expression of p-p38 vs. CD61 on gated CD14hi monocytes post chamber.

Table 1:

CyTOF Antibody Panels

Surface Staining Panel			
Isotope	**Target**	**Clone**	**Source**
113 In	CD57	HCD57	Biolegend
115 In	CD45	HI130	Biolegend
141 Pr	CD235a/b	HIR2	Fluidigm
142 Nd	CD19	HIB19	Biolegend
143 Nd	CD45RA	HI 100	Biolegend
145 Nd	CD4	RPA-T4	Biolegend
146 Nd	CD8	RPA-T8	Biolegend
148 Nd	CD16	3G8	Biolegend
149 Sm	CD127	A019D5	Biolegend
150 Nd	CD1c	L161	Biolegend
151 Eu	CD123	6H6	Biolegend
152 Sm	CD66b	G10F5	Biolegend
155 Gd	CD27	0323	Biolegend
160 Gd	CD14	M5E2	Biolegend
161 Dy	CD56	B159	Biolegend
166 Er	CD25	M-A251	Biolegend
168 Er	CD3	UCHT1	Biolegend
170 Er	CD38	HB-7	Biolegend
171 Yb	CD161	HP-3G10	Biolegend
174 Yb	HLADR	L243	Biolegend
209 Bi	CD61	VI-PL2	Fluidigm
Intracelluar Phosphoprotein Panel			
Isotope	**Target**	**Clone**	**Source**
147 Sm	p-STAT5	47	Fluidigm
153 Eu	p-STAT1	58D6	Fluidigm
156 Gd	p-p38	D3F9	Fluidigm
158 Gd	p-STAT3	4	Fluidigm
159 Tb	p-MAPKAP2	27B7	Fluidigm
162 Dy	p-PLCg2	K86–689.37	Fluidigm
164 Dy	IkBa	L35A5	Fluidigm
165 Ho	p-CREB	87G3	Fluidigm
167 Er	p-ERK1/2	D13.14.4E	Fluidigm
175 Lu	p-S6	N7–548	Fluidigm

Table 2:

Thromboelastometry and thrombus area results

	Healthy control (n=23)	SCD (n = 5)	P value
Age, median (range)	29 (26–32)	29 (26–32)	NA *
Gender (% male)	80%	80%	NA *
Thrombus area, low shear μm^2 -median (range)	6217 (4984 – 6832)	7250 (5541 – 8971)	0.001
Thrombus area, high shear μm^2 -median (range)	13559 (11329 – 15005)	11124 (10269 – 12907)	0.08
Intrinsic TEM - median (range)			
CT	149 (146 – 174)	163 (116 – 200)	0.73
A5	42 (35 – 48)	52 (30 – 60)	0.04
A30	63 (55 – 63)	67 (52 – 74)	0.05
CFT	78 (68 – 123)	55 (44 – 157)	0.04
MCF	62 (54 – 64)	67 (52 – 74)	0.04
MCF-t	1875 (1322 – 2149)	1441 (1200 – 1945)	0.05
Alpha angle	76 (67 – 77)	79 (63 – 81)	0.04
CFR	76 (68 – 79)	80 (63 – 82)	0.05
MCE	171 (146 – 178)	206 (108 – 281)	0.05
G	8544 (7315 – 8914)	10302 (5402 – 14060)	0.05
TPI	68 (36 – 81)	111 (21 – 192)	0.05
MAXV	17 (10 – 20)	22 (8 – 29)	0.04
MAXVt	170 (158 – 203)	197 (148 – 216)	0.6
AUC	6135 (5379 – 6323)	6689 (5159 – 7329)	0.04
Extrinsic TEM - median (range)			
CT	65 (50 – 66)	102 (89 – 113)	0.00
A5	43 (34 – 46)	52 (32 – 61)	0.04
A30	64 (56 – 66)	66 (54 – 72)	0.4
CFT	96 (78 – 149)	55 (46 – 147)	0.02
MCF	65 (52 – 66)	66 (54 – 72)	0.19
MCF-t	1934 (1636 – 2197)	1438 (952 – 1878)	0.00
Alpha angle	71 (62 – 75)	79 (63 – 80)	0.02
CFR	75 (68 – 77)	80 (68 – 81)	0.02
MCE	180 (124 – 195)	198 (117 – 254)	0.23
G	9013 (6169 – 9756)	9925 (5863 – 12706)	0.29
TPI	62 (25 – 75)	112 (24 – 165)	0.05
MAXV	15 (10 – 17)	24 (10 – 27)	0.02
MAXVt	117 (84 – 151)	127 (121 – 155)	0.09
AUC	6398 (5182 – 6691)	6593 (5381 – 7123)	0.52

* P values not calculated because participants were age and gender matched to controls

Abbreviations for Table 2:

Acronym	Parameter	Definition	Unit
Suggested Routine Parameters for ROTEM® Analysis are shaded			
CT	Coagulation Time (syn. IFT, r)	The time after which a 2 mm amplitude had been reached	sec
A5	Firmness at time 5 minutes		
A30	Firmness at time 30 minutes		
CFT	Clot Formation Time (20 mm)	The time between 2 mm amplitude and 20 mm amplitude	sec
MCF	Maximum Clot Firmness	The maximum amplitude reached	mm
	(syn. MA)		
MCF-t	MCF-Time	The time from CT till MCF had been reached	sec
a	a-Angle	A tangent to the clotting curve through the 2 mm point.	degree(°)
CFR	Clot Formation Rate (°)	The secant at the maximum slope	degree(°)
MCE	Maximum Clot Elasticity E=100*MCF/(100-A)	MCE (maximum clot elasticity) is a calculated parameter. It is a normalised elastic scale in which a normal clot (50 mm MCF) is assigned an elastic modulus of 100.	
G	G 5000MCF/(100-MCF) (Elastic shear modus)	G is the shear elastic modulus strength, a calculated parameter. It increases exponentially as compared to the amplitude. It allows a more sensitive	
		resolution at high amplitudes. G= (5000 * MCF)/(100-MCF)	
	Thrombodynamic Potential In- dex.	According to the author (Raby) Thrombodynamic Potential Index describes the patient's global coagulation.	
TPI	TPI = EMX/K EMX (100*MCF)/100-MCF)		
Research parameters for derivative curves (according to B. Sorensen et al. 2003)			
maxVel*	Max. of 1st derivative	The maximum of the 1st derivative of the clot curve	
t-maxVel*	Time to achieve max of 1 st derivative	Time from reaction start to reach the maximum velocity	sec
AUC*	Area under 1 st derivative curve. Ends at MCF	AUC is defined as the area under the velocity curve from the start of the measurement until the time AUC-t has been reached. The numerical value is multiplied by 60.	mm × 60

Table 3:

Participant Characteristics

Characteristic	Healthy Control (n=3)	Sickle Cell Disease (n=4)
Age (median (range))	57 (47 – 65)	28 (26 – 32)
Gender (% male)	33.3%	100%